Higher harmonic inverse free-electron laser interaction

P. Musumeci,[1] C. Pellegrini,[2] and J. B. Rosenzweig[2]
[1]*Dipartimento di Fisica and INFN, Università di Roma "La Sapienza," Piazzale Aldo Moro 2, 00185 Rome, Italy*
[2]*Department of Physics and Astronomy, UCLA, Los Angeles, California 90095, USA*
(Received 31 January 2005; published 8 July 2005)

We expand the theory of the inverse free electron laser (IFEL) interaction to include the possibility of energy exchange that takes place when relativistic particles traversing an undulator interact with an electromagnetic wave of a frequency that is a harmonic of the fundamental wiggler resonant frequency. We derive the coupling coefficients as a function of the IFEL parameters for all harmonics, both odd and even. The theory is supported by simulation results obtained with a three-dimensional Lorentz equation solver code. Comparisons are made between the results of theory and simulations, and the recent UCLA IFEL experimental results where higher harmonic IFEL interaction was observed.

DOI: 10.1103/PhysRevE.72.016501 PACS number(s): 41.60.Cr, 41.75.Jv, 41.75.Lx

I. INTRODUCTION

With the simultaneous availability in many research laboratories around the world of very high power laser systems and high quality relativistic electron beams, a variety of techniques has been developed in order to provide efficient energy and/or information exchange between the electrons and the photons. One of the most successful solutions to this problem is the inverse free-electron laser (IFEL) interaction [1,2]. In an IFEL, relativistic electrons copropagate with a laser beam through an undulator magnet. The undulator produces a small, oscillatory transverse velocity (wiggling motion) in a direction parallel to the electric vector of the electromagnetic wave so that energy can be transferred from the wave to the particles. Efficient energy exchange takes place when the electron phase slippage in the wave is such that its transverse velocity changes sign synchronously with the laser field (resonant condition [3]).

Together with the natural appeal of using the ultrahigh electric field of an intense laser beam to accelerate the electrons, the IFEL scheme offers the possibility to manipulate the electron longitudinal phase space on the time scale of the laser wavelength. Successful experimental demonstrations achieved with the IFEL scheme include the microbunching of the electron beam [4], the phase-locking of an electron microbunch train with a laser wave [5,6], and, recently, the high gradient acceleration of electrons [7].

There are a wide variety of proposed schemes and experiments involving laser and electron beam coupling that rely ultimately on the IFEL mechanism: the modulator sections in (FEL) high-gain harmonic-generation [8], advanced accelerator prebunchers [9,10], compact laser injectors for x-ray FELs [11], electron beam current enhancer [12], optical stochastic cooling [13], and laser slicing methods [14]. For each of these applications, it is of fundamental importance to understand and optimize the coupling and the efficiency of the energy exchange between the laser wave and the electrons.

The IFEL resonance condition is ordinarily understood to mean that efficient energy exchange between the transverse EM wave and the electrons can only take place at electron energies such that, in the electron rest frame, the wiggling induced by the laser has the same frequency as the wiggling induced by the undulator. However, when the motion in the electron rest frame is not a simple dipole oscillation, resonance can also occur if the laser frequency is a *multiple* of the undulator wiggling frequency, that is, electrons of a fixed energy may interact not only with the fundamental radiation frequency but also with its harmonics [15]. From an alternative point of view, particles of different energies $\gamma_{r,n}$ can interact with the same laser frequency because they see the EM wave as a higher harmonic of the fundamental frequency which they are resonant with. In other words, for a given laser wavelength and undulator magnet, there are multiple resonant energies

$$\gamma_{r,n} = \sqrt{\frac{\lambda_w(1+K^2/2)}{2n\lambda}}, \tag{1}$$

where λ_w is the undulator period, K is the normalized undulator amplitude, and λ the radiation wavelength.

The higher harmonic interaction can be viewed as the natural consequence of the fact that the spectrum of the spontaneous radiation emitted by a relativistic electron passing through a planar undulator magnet presents peaks at different frequencies that are harmonics of a fundamental resonant frequency. In a quantum mechanic description of the interaction, because of the presence of these strong lines in the spontaneous radiation spectrum, stimulated emission (FEL emission at higher harmonics) or absorption (higher harmonic IFEL) of radiation at these frequencies is possible.

In the FEL literature, significant power at the harmonics of the undulator resonant frequency has been both theoretically investigated [16] and then experimentally observed [17]. Even though the possibility of IFEL harmonic coupling follows directly from these results and even though the simple one-dimensional theoretical model description allows for IFEL harmonic interaction, most of the IFEL literature and experiments have only considered coupling the laser and the relativistic electron beam at the fundamental undulator resonant frequency. Future proposals involving IFEL schemes foresee the same coupling.

In this paper, we study in detail the possibility of IFEL interaction between a relativistic electron beam and a high

power laser beam with a frequency that is a *harmonic* of the undulator fundamental resonant frequency. In the following section, we derive the coupling coefficients for all the harmonics. We obtain, as expected from symmetry considerations, that even-harmonic coupling is suppressed in a perfectly aligned system. We show in the third section at least two possibilities in which the symmetry is broken and even-harmonic coupling becomes non-negligible. Numerical simulations obtained with the three-dimensional code TREDI confirm the results of the analytic calculations.

We then explore the possibilities opened up by this coupling scheme showing that the higher harmonic interaction adds flexibility and a new degree of freedom—the harmonic number n—in the design of systems capable of coupling relativistic electron beams and high power laser beams. We apply our calculations to two practical examples where the harmonic coupling can be important. We discuss a IFEL microbuncher where the higher harmonic interaction can ease the undulator design, and in some cases be competitive with the usual fundamental frequency IFEL coupling. In a second case we analyze the effects of the higher harmonic coupling in an IFEL accelerator where the undulator is strongly tapered to compensate for the change in electron energy. The study of this case allows us to benchmark the theory and the simulations with experimental data from the recent Neptune IFEL accelerator experiment, where the higher harmonic IFEL interaction was first observed.

II. THEORY

To derive the higher harmonic IFEL equations of motion we will closely follow the arguments that lead to the formulation of the IFEL equations in [2]. Neglecting the effect of the electron current on the evolution of the radiation (assumption valid in the limit of very small beam charge), the IFEL interaction can be described by the equations that govern the electron motion in the combined field of an electromagnetic plane wave of a given frequency ω and a planar wiggler magnetic field,

$$m\frac{d(\gamma \boldsymbol{v})}{dt} = e\left[\boldsymbol{E_l} + \frac{\boldsymbol{v}}{c} \times (\boldsymbol{B_l} + \boldsymbol{B_w})\right], \tag{2}$$

where $\boldsymbol{E_l}=[E_0 \cos(kz-\omega t+\phi),0,0]$ and $\boldsymbol{B_l}=\hat{\boldsymbol{z}}\times\boldsymbol{E_l}$ are the electric and magnetic fields of the plane wave, $\boldsymbol{B_w}=[0,B_0 \cos(k_w z),0]$ is the magnetic field of the wiggler (in-symmetry plane approximation), and $\gamma=(1-\beta^2)^{-1/2}$, $\boldsymbol{\beta}=\boldsymbol{v}/c$ are the familiar relativistic factors.

We can easily determine the transverse velocity if we observe that, in this simple case for the external fields, the transverse canonical momentum is conserved:

$$\mathbf{p_T} = m\gamma \mathbf{v_T} + e(\mathbf{A}_l + \mathbf{A}_w) = \text{const}, \tag{3}$$

where $\mathbf{A}_l$ and $\mathbf{A}_w$ are the vector potentials, respectively, of the laser and the wiggler fields. The constant is equal to the value of the transverse momentum outside the undulator and the laser fields. For electrons entering the interaction region parallel to the laser propagation axis, the constant is equal to zero.

We can introduce the normalized vector potential amplitudes $K=eB_0/mck_w$ and $K_l=eE_0/mc^2k$ and note that, because the large wavelength difference between the laser field and the undulator field, for typical values of the laser electric field and the magnetic field amplitude, we have $K \gg K_l$. We can then use the approximation that the electron transverse motion is dominated by the magnetic field of the undulator, and write for the electron velocity the expression

$$\boldsymbol{\beta} = \left(\frac{K}{\gamma}\cos(k_w z) - \theta, 0, \sqrt{1 - \frac{1 + K^2\cos^2(k_w z) - 2\theta\gamma K\cos(k_w z) + \gamma^2\theta^2}{\gamma^2}}\right), \tag{4}$$

where θ is the angle in the horizontal plane formed by directions of propagation of electrons and laser beam and, consistently with the undulator field expression, we have restricted ourselves to the study of the electron motion in the symmetry plane of the magnet $y=0$. The latter is justified by the fact that the electron motion in the vertical direction is uncoupled from the horizontally polarized electromagnetic wave and its only effect for the IFEL interaction would be a modification of the longitudinal component of the velocity [i.e., $\gamma^2\theta^2=\gamma^2(\theta_x^2+\theta_y^2)$].

The energy transferred between the laser beam and electron per unit length of the accelerator is given by

$$\frac{d\gamma}{dz} = \frac{e}{mc^3}v_x E_x = kK_l\left[\frac{K}{2\gamma}(\sin\psi_+ + \sin\psi_-) - \theta\sin(kz-\omega t)\right], \tag{5}$$

where $\psi_\pm=(k\pm k_w)z-\omega t$. The terms oscillating at the EM wave frequency in Eq. (5) have a very small effect on the electron dynamics and will be neglected. Using the z component of Eq. (4) and $\gamma \gg 1$, one can express the time t as a function of the distance z,

$$ct = ct_0 + z + \int_0^z dz\frac{2+K^2+2\gamma^2\theta^2}{4\gamma^2} + \frac{1}{8}\frac{K^2}{\gamma^2 k_w}\sin(2k_w z) - \frac{K\theta}{\gamma k_w}\sin(k_w z). \tag{6}$$

The last terms are approximations for $\frac{1}{4}\int_0^z dz(K^2/\gamma^2)\cos(2k_w z)$ and $\int_0^z dz(K\theta/\gamma)\cos(k_w z)$, respectively. These approximations are valid when the changes of all the system parameters over one wiggler period are small.

Using the expansion

$$\sin(a + b\sin\phi + c\sin\Phi) = \sum_{m=-\infty}^{\infty}\sum_{p=-\infty}^{\infty} J_p(b)J_m(c) \times \sin(a + p\phi + m\Phi), \tag{7}$$

where J_n are Bessel functions, in the expression for $\sin\psi_+ + \sin\psi_-$, we obtain

$$\sin\psi_+ + \sin\psi_- = \sum_{m=-\infty}^{\infty}\sum_{p=-\infty}^{\infty} J_m(G)J_p(\xi)\sin\left[k_w z(2m+p+1) - k\int_0^z dz\frac{2+K^2+2\gamma^2\theta^2}{4\gamma^2} - \phi_0\right] + J_m(G)J_p(\xi)\sin\left[k_w z(2m+p-1) - k\int_0^z dz\frac{2+K^2+2\gamma^2\theta^2}{4\gamma^2} - \phi_0\right], \quad (8)$$

where $G=kK^2/8k_w\gamma^2$ and $\xi=kK\theta/\gamma k_w$.

We can then collect the terms that have the same phase nk_wz and changing the summation indexes, we get

$$\sin\psi_+ + \sin\psi_- = \sum_{n=-\infty}^{\infty}\sum_{m=-\infty}^{\infty}\{J_m(G)[J_{2m+n+1}(\xi) + J_{2m+n-1}(\xi)]\}\sin\left[k_w zn - k\int_0^z dz\frac{2+K^2+2\gamma^2\theta^2}{4\gamma^2} - \phi_0\right]. \quad (9)$$

For a small angle between the electron beam and the laser propagating directions ($\xi \ll 1$ or $\theta \ll \gamma k_w/kK$), we can expand the Bessel function for small arguments and Eq. (9) can be approximated by

$$\sin\psi_+ + \sin\psi_- = \sum_{n=-\infty}^{\infty} \mathrm{JJ}_n^*\sin\left[k_w zn - k\int_0^z dz \times\frac{2+K^2+2\gamma^2\theta^2}{4\gamma^2} - \phi_0\right], \quad (10)$$

where

$$\mathrm{JJ}_n^* = (-)^{(n-1)/2}[J_{(n-1)/2}(G) - J_{(n+1)/2}(G)] \quad \text{for } n \text{ odd}$$

$$= (-1)^{(h+1)/2}\xi[J_{(n-2)/2}(G) - J_{(n+2)/2}(G)] \quad \text{for } n \text{ even}. \quad (11)$$

Efficient energy exchange can occur only for those terms in the sum for which the argument of the sine function $\psi + (n-1)k_wz$ is slowly varying with $\psi = k_wz - k\int_0^z dz[(2+K^2)/4\gamma^2] - \phi_0$. The accelerator can be designed in such a way that only one term of all those appearing in the summation in Eq. (10) is important because of its slow variation along the accelerator. For example in the case in which the $n=1$ term is relevant, we recover the usual fundamental IFEL accelerator equations

$$\frac{d\gamma}{dz} = \frac{kK_lK}{2\gamma}\mathrm{JJ}\sin\psi, \quad (12a)$$

$$\frac{d\psi}{dz} = k_w - k\frac{1+K^2/2}{2\gamma^2}, \quad (12b)$$

where $\mathrm{JJ}=[J_0(G)-J_1(G)]$ and $G \simeq K^2/(4+2K^2)$.

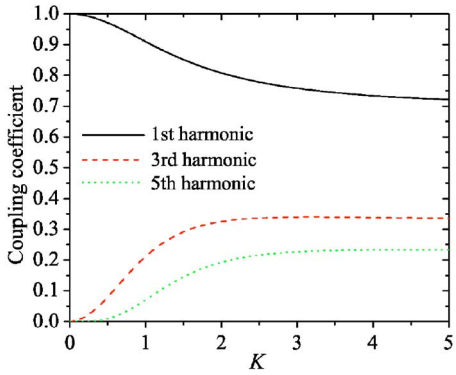

FIG. 1. (Color online) Coupling coefficients JJ_n for $n=1,3,5$ vs K.

This case corresponds to demanding that the derivative of the ponderomotive phase ψ vanishes, that is

$$k_w - k_0\frac{1+\frac{K^2}{2}}{2\gamma_r^2} = 0, \quad (13)$$

where $k_0=\omega_0/c$ is the fundamental resonant wave number. At a closer look, this is merely an equivalent way of writing the condition (1) for $n=1$.

If we now consider the terms with $n \neq 1$ we have

$$\frac{d\gamma}{dz} = \frac{kK_lK}{2\gamma}\sum_n \mathrm{JJ}_n\sin[\psi + k_wz(n-1)], \quad (14a)$$

$$\frac{d\psi}{dz} = k_w - k\frac{1+K^2/2+\gamma^2\theta^2}{2\gamma^2}, \quad (14b)$$

where JJ_n are the coupling coefficients for the nth harmonic and are given by

$$\mathrm{JJ}_n = \sum_{m=-\infty}^{+\infty} J_m(G)[J_{2m+n+1}(\xi) + J_{2m+n-1}(\xi)]. \quad (15)$$

It is not surprising, because of the symmetry of the radiation emission and absorption processes, that these coefficients have been already derived in the parallel FEL literature by Colson and Dattoli [18] in the calculation of the power radiated by a relativistic electron beam in the harmonics of the fundamental wiggler frequency.

To find the terms that have a quasiconstant phase and can yield a net contribution to the energy change of the particles, we take the derivative of the argument of the sine function in Eq. (14a)

$$\frac{d}{dz}[\psi + k_wz(n-1)] = nk_w - k\frac{1+\frac{K^2}{2}}{2\gamma^2} = 0. \quad (16)$$

Maintaining the same undulator parameter and electron beam energy, all the electromagnetic waves with frequency $\omega = n\omega_0$ can efficiently exchange energy with the electron beam.

In Fig. 1 we show the calculated coupling coefficients for

the odd harmonics as a function of K for a planar undulator. In the next section we will discuss the mechanism of coupling with the even harmonics.

For very small K (undulator magnet) the first harmonic IFEL interaction is dominant. For larger values of K the other coefficients grow to finite values and significant energy exchange can happen via higher harmonic IFEL interaction.

III. EVEN-HARMONIC COUPLING

It is known that the on-axis spectral content of the planar undulator radiation presents peaks only at the odd harmonics. The even harmonics, in fact, are suppressed by the symmetry of the radiation emitting source. Only off-axis, the even harmonic radiation is present.

Correspondingly, in the IFEL interaction, when the angle θ between the particles and the plane wave tends to zero, the strength of the interaction between the relativistic electrons and the even-harmonics radiation also vanishes. Mathematically, this can be stated as

$$\lim_{\xi \to 0} \mathrm{J}\mathrm{J}_n(G,\xi) = 0 \quad \text{for } n \text{ even}. \tag{17}$$

This can be understood more clearly if one examines the acceleration of an electron during a single period of oscillation inside the wiggler (i.e., before period averaging). In Fig. 2(a) we show the maximum beam energy as a function of distance along the undulator for the first three harmonic IFEL interactions. In the simulations, the beam injection energy has been tuned to the resonant values relative to the different higher harmonic IFEL interactions, maintaining the same undulator and laser parameters. Also shown is the wiggling beam trajectory [Fig. 2(c)]. It is clear that, as could be deduced by an inspection of Eq. (5), the energy exchange occurs in the regions where the electron transverse velocity is nonvanishing and can couple to the transverse electric field of the laser (not shown). When the first harmonic resonance condition is satisfied the electrons slip back in phase with respect to the laser one radiation wavelength per undulator period. In such a way, at the end of each period the phase relationship is conserved and there is a net acceleration. When the third harmonic resonance condition is satisfied, the electrons slip back three laser wavelengths for each undulator period. Also in this case, there can be a net energy gain for the electrons. When the electrons slip an even number of periods with respect to the laser wave, though, the energy gained from the laser field in the first half of the trajectory is subtracted in the interaction with an equal and opposite field in the following part of the oscillation period, so that the net energy gain is null. A similar argument for higher even-harmonic IFEL interactions also dictates that they vanish due to the cancellation of acceleration and deceleration over a period.

In order to obtain finite coupling with the even-harmonics, it is necessary to find a mechanism which breaks the symmetry of acceleration and deceleration portions of the undulator period. In the previous section we discussed one obvious possibility for such a mechanism. If there is an angle between the direction of propagation of the laser and the incoming electron beam, there is a preferred direction for the electrons to interact with the laser, and the amount of energy gained in the first half of the oscillation period is not perfectly compensated by the energy lost in the other half [see Fig. 2(b)].

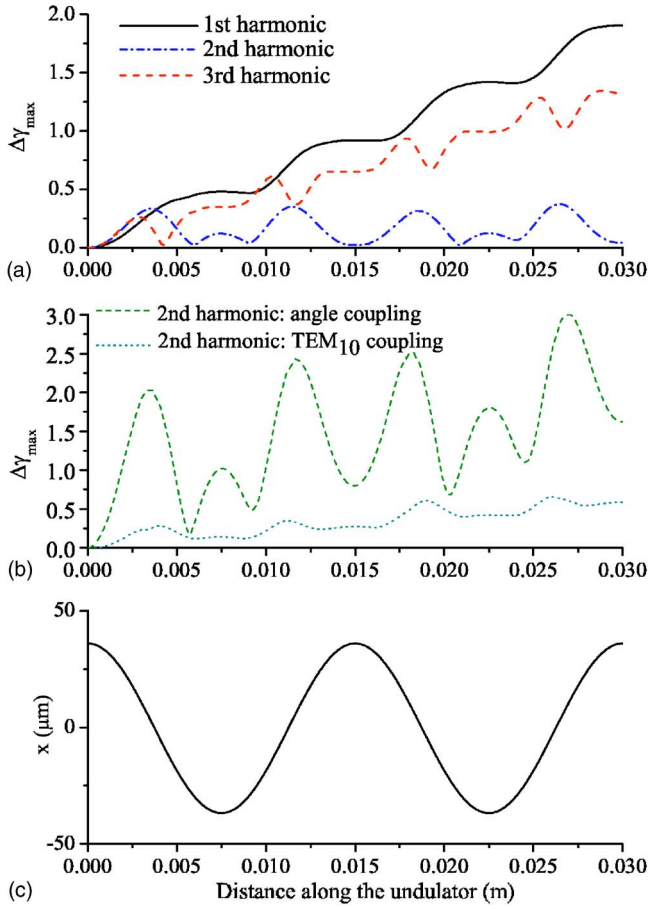

FIG. 2. (Color online) (a) Maximum energy gain (in units of mc^2) for an electron beam interacting with electromagnetic waves at the first three IFEL resonant frequencies, followed through two wiggler periods. (b) Maximum energy gain (in units of mc^2) for two coupling schemes with non-negligible second harmonic IFEL interaction. (c) Electron beam trajectory inside the wiggler.

Let us consider a practical example, an electron beam interacting with an electromagnetic plane wave of wavelength $\lambda = 1.06\ \mu$m inside an undulator with period $\lambda_w = 1.5$ cm and normalized magnetic amplitude $K = 3$. The fundamental resonant energy in this case is $\gamma_{r,1} = 200$. To have a finite even-harmonic IFEL coupling, we introduce a small angle θ between the electron beam and the laser propagating directions. Note that the resonant energies are a function of this crossing angle,

$$\gamma_{r,n}(\theta) = \sqrt{\frac{\lambda_w}{2n\lambda - \lambda_w\theta^2}\left(1 + \frac{K^2}{2}\right)}. \tag{18}$$

In particular, for the second harmonic IFEL interaction, when $\theta = 2$ mrad, we have $\xi \cong 0.6$ and the coupling coefficient is $\mathrm{J}\mathrm{J}_2 \cong 0.23$, which is small but certainly not negli-

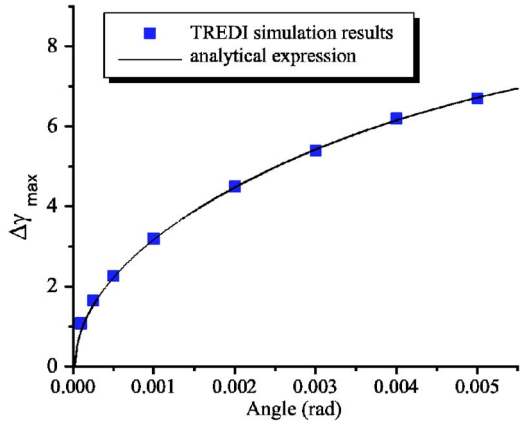

FIG. 3. (Color online) Maximum energy gain (in units of mc^2) for second harmonic IFEL interaction vs input angle.

gible when compared to the fundamental coupling $JJ_1 = 0.73$.

With the help of the three-dimensional simulation code that we will describe more in detail in the next section, we have verified the coupling coefficient analytical estimates. In Fig. 3, the maximum energy gain for electrons injected in an undulator tuned on the second harmonic IFEL resonance [$\gamma = \gamma_{r,2}(\theta)$] is shown as a function of the crossing angle θ. The laser intensity in these simulations is 3×10^{13} W/cm^2. Note that the maximum energy gain corresponds to the height of the separatrix in the longitudinal phase space. This can be written in terms of the relevant parameters of the IFEL interaction as [3]

$$\frac{\delta\gamma_{\max}}{\gamma} = \sqrt{\frac{2K_l K \mathrm{JJ}_n}{1 + \frac{K^2}{2}}}. \tag{19}$$

It is thus proportional to the square root of the coupling coefficient. The simulation results (dots) agree quite well with the theoretical prediction (line).

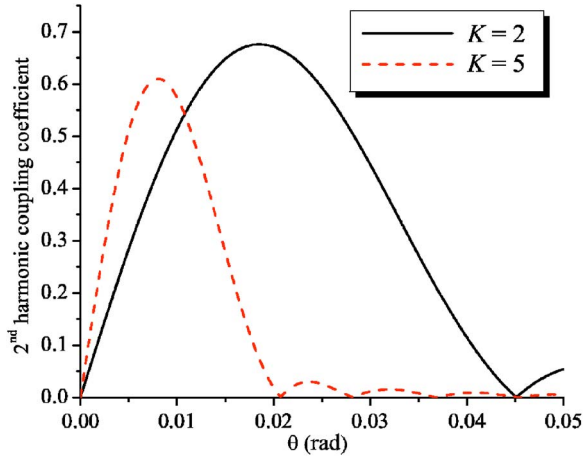

FIG. 4. (Color online) Coupling coefficient for second harmonic IFEL interaction vs θ.

It is instructive to see how the coupling coefficient for the even harmonics depends on the value of the crossing angle θ. In Fig. 4 we show JJ_n with $n=2$ evaluated as a function of θ for two different values of K. The first thing to notice is that the coupling can be significant (up to 0.7). A second relevant observation derived from Fig. 4 is that for a stronger undulator (larger K) coupling to harmonics occurs for a smaller value of the crossing angle θ. This is in general true for all the coupling coefficients as is seen also in Fig. 1. Coupling to higher harmonic is favored by a stronger (larger K) undulator.

The symmetry that suppresses the even-harmonic interaction can be also broken when we consider the interaction of the electrons with a laser mode having odd symmetry in the oscillation plane, for example, a Hermite-Gaussian TEM_{10} mode. In this case, when an even harmonic resonance condition is satisfied, the electrons can experience a net gain energy because the laser field changes sign crossing the axis [see Fig. 2(b)]. This is the inverse counterpart of the well-known fact that the even-harmonic radiation emitted by one electron traveling through an undulator presents an odd symmetry profile in the wiggling plane [19].

The electric field component of a Hermite-Gaussian laser mode can be written as [20]

$$\frac{E_{mn}}{E_0} = \frac{w_0}{w(z)} H_m\left(\frac{\sqrt{2}x}{w(z)}\right) H_n\left(\frac{\sqrt{2}y}{w(z)}\right) e^{-(x^2+y^2)/w(z)^2} \cos\phi_{mn}, \tag{20}$$

where the spot size evolution is

$$w(z) = w_0 \sqrt{1 + \left(\frac{z - z_w}{z_r}\right)^2}, \tag{21}$$

and the phase is given by

$$\phi_{mn} = kz + \frac{x^2 + y^2}{w(z)^2}\frac{z}{z_r} - (m + n + 1)\arctan\left(\frac{z}{z_r}\right). \tag{22}$$

Let us consider a mode that has an odd symmetry in the oscillation plane, the TEM_{10} mode, where $H_0 = 1$ and $H_1(x) = 2x$.

Substituting the mathematical form for this mode into the expression for the rate of energy exchange, at first order in the transverse displacement from the axis, we obtain (assuming $\theta = 0$)

$$\frac{d\gamma}{dz} = \frac{kK_l(z)K}{2\gamma}\frac{K\sqrt{2}}{k_w \gamma w(z)} \sin(2k_w z)\sin(kz - \omega t). \tag{23}$$

By the use of the trigonometric identities, Eq. (6) for the time t, and the Bessel function expansion (7) we can rewrite Eq. (23) as

$$\frac{d\gamma}{dz} = \frac{kK_l(z)K}{2\gamma} \sum_{\text{even n}} \mathrm{JJ}_n^* \sin[\psi + k_w z(n-1)], \tag{24}$$

with JJ_n^* given by the same expression (for the even n) as Eq. (11), where now

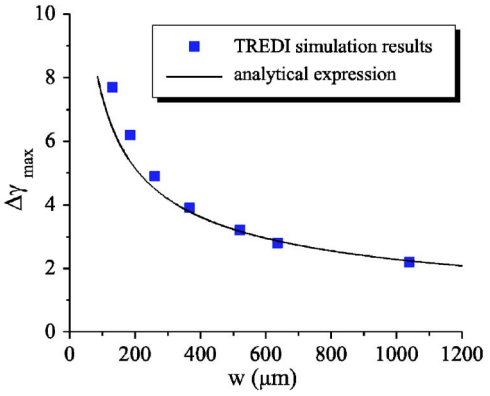

FIG. 5. (Color online) Maximum energy gain (in units of mc^2) for second harmonic IFEL interaction vs spot size of TEM_{10} mode.

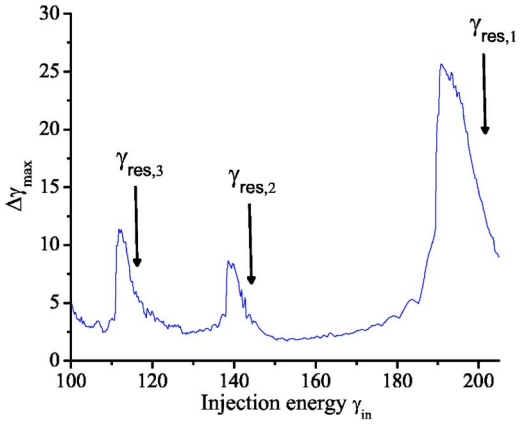

FIG. 6. (Color online) Maximum energy gain (in units of mc^2) of particles injected in a IFEL accelerator at different energies. The vertical arrows indicate the higher harmonic IFEL resonant energies $\gamma_{r,n}$ with $n=1,2,3$.

$$\xi = \frac{K\sqrt{2}}{k_w \gamma w(z)}. \tag{25}$$

The parameter ξ is the ratio between the transverse wiggling amplitude of the electron beam to the laser beam size [19]. Note that in this case it is not physically relevant to extrapolate this result for $\xi > 1$, since in this case the electrons would oscillate out of the region where the electromagnetic field is present.

Again, we consider a reference case with an electron beam with energy $E=72$ MeV (tuned at the second harmonic IFEL resonance) interacting with a TEM_{10} laser mode of wavelength $\lambda=1.06$ μm and power $P=100$ GW, inside an undulator with period $\lambda_w=1.5$ cm and normalized magnetic field amplitude $K=3$. For a Hermite-Gaussian modal parameter $w=130$ μm, from Eq. (25) we obtain $\xi=0.56$ and $JJ_2=0.208$.

The analytical estimates are benchmarked against the results from the three-dimensional simulations. In Fig. 5 we show the maximum energy of the electrons as a function of the spot size parameter w of the TEM_{10} mode. For small spot sizes w, we observe some differences in the maximum energy gain between the simulation results and the value calculated from the analytical estimate of the coupling coefficient. These discrepancies are due to the fact that when the Rayleigh range is very short, the stable ponderomotive bucket is disrupted by the sharp Guoy phase shift experienced by the laser mode going through the focus [21]. In such cases the maximum energy gain no longer corresponds to the ponderomotive bucket height. In fact, the bucket height itself is not a valid concept in this scenario, as the parameters of the Hamiltonian describing the interaction change too quickly.

Generally the coupling to the even harmonics is also nonzero whenever the electrons sample a gradient of the electromagnetic wave intensity during the oscillation around the axis and the symmetry is broken. This is the case, for example, when there is a transverse offset of the beams trajectories or hot spots in the electromagnetic transverse profile are present. These forms of coupling are to be avoided, however, because they mix horizontal and longitudinal phase spaces and introduce unwanted correlations that are difficult to eliminate afterwards.

IV. SIMULATIONS

In order to model the IFEL interaction we employed the TREDI simulation code [22]. The code pushes the particles using the Lorentz equation of motion with a fourth order Runge-Kutta integration method in a three-dimensional Cartesian reference frame under the influence of arbitrary external fields. In its IFEL version [21], it is used to simulate the motion of the electrons in the combined field of an undulator magnet, represented with a three-dimensional magnetic field map and a laser wave, given by an analytical expression representing the sum of Hermite-Gaussian modes.

The code is self-consistent since it computes the electron self-fields based on the Lienard-Wiechert based formalism. Calculating both the velocity and the radiation components of the electromagnetic fields generated by each particle, the code takes into account the important collective effects of the space charge and of coherent radiation emission on the electron dynamics. Estimates of these effects can be also found in the literature [23,24]. For a higher harmonic IFEL interaction in particular it is necessary to keep in mind that the ponderomotive potential amplitude is reduced with respect to the fundamental IFEL interaction because of a smaller higher harmonic coupling coefficient. This in practice reduces the amount of charge in one ponderomotive bucket before the collective effect starts to make a significant contribution to the longitudinal electron motion. For example, in the reference cases discussed in the previous section with a driving laser of wavelength $\lambda=1.06$ μm, we found that the collective effects for the second harmonic interaction are negligible provided that the peak electron current is less than 0.5 kA, or equivalently that the amount of charge in one microbunch is less than 0.1 pC. In what follows we assume a beam current low enough that both space charge and coherent radiation emission effects are negligible. Because of this, the CPU-

time-intensive Lienard-Wiechert calculation is turned off in the TREDI simulations.

Since the code solves the Lorentz equations and it does not suffer from any approximation due to the period-averaging of the equations, we can check the analytical calculations of the IFEL coupling coefficients against the numerical solution for the electron motion. In Fig. 6 the energy gain of electrons with different initial energies, injected with a small angle $\theta=1$ mrad inside an undulator with a 1.5 cm period and a normalized magnetic amplitude $K=3$ interacting with an electromagnetic wave of wavelength $\lambda=1.06$ μm and intensity 10^{13} W/cm^2, is displayed.

Multiple peaks near the energies corresponding to the different higher harmonic IFEL interactions (vertical arrows) are observed in these simulations. The peaks correspond to the regions where the interaction is stronger and an analysis of the longitudinal phase spaces for the region of injection energies around the peaks shows the existence of stable ponderomotive buckets. Note that the maximum energy gain, as expected, reaches a larger value when the electrons are injected with energy slightly below the resonant energy value. In this case, in fact, the particles rotate in the longitudinal phase space from the bottom of the ponderomotive bucket to the top and gain almost twice as much energy. The amount of energy gain of the electrons observed in the three-dimensional simulations corresponds well to the height of the ponderomotive buckets that can be calculated from Eq. (19) using the coupling coefficients given in Eq. (15).

V. IFEL MICROBUNCHER

Keeping in mind the possibility of the higher harmonics IFEL interaction, we next turn our attention to the problem of designing an IFEL buncher for a given laser wavelength and electron beam energy. Such a device is used, for example, in advanced accelerators in order to decrease the final energy spread of a short wavelength high gradient accelerator, injecting a phase-locked train of microbunches with the same periodicity of the accelerating wave [6,9,10]. The same device finds also applications in light sources laboratories, as the modulator section in FEL seeding experiments. The seed radiation in this scheme interacts with the relativistic electrons in a section of the undulator and imparts an energy modulation on the electron beam that a subsequent dispersive section turns into spatial microbunching [8].

An IFEL buncher undulator and a FEL modulator section are usually tuned so that the radiation wavelength corresponds to the fundamental resonant frequency of the undulator. On the other hand, the energy of the electron beam is normally constrained by the available radiofrequency accelerator. Building an undulator with the parameters required to match the fundamental resonant frequency to the laser wavelength available can often be an unfeasible task, especially for lower beam energies. It is in these situations that the use of the higher harmonic IFEL interaction to couple the electrons and the photons can be very effective.

Another important and related point is that coupling to a higher harmonic electromagnetic wave means that the normalized amplitude K of the IFEL undulator can be larger.

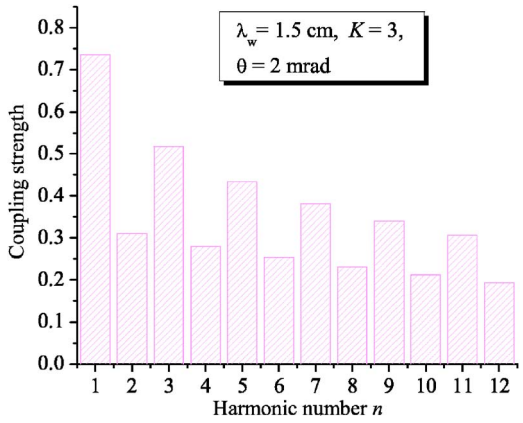

FIG. 7. (Color online) Coupling strength $K\,\mathrm{JJ}_n(K)$ vs harmonic number n.

Assuming $K^2/2 \gg 1$ and satisfying the resonant condition (1), when we couple a beam of fixed energy and the laser through the nth harmonic interaction, K can be larger by a factor $\sqrt{n}$. The important parameters of the IFEL interaction, such as the synchrotron frequency and the height of the ponderomotive bucket depend on the square root of the coupling strength $K\mathrm{JJ}_n(K)$ [3]. A higher coupling strength implies a higher frequency of the longitudinal phase space rotation which makes the IFEL a stronger longitudinal lens.

We show in Fig. 7 the coupling strength $K\mathrm{JJ}_n(K)$ as a function of the harmonic number for the test case with $K=3$, $\lambda_w=1.5$ cm, $\gamma_{r,1}=200$, and $\theta=2$ mrad. The coupling decreases with the harmonic number n so that the fundamental coupling is always more efficient, but because of its slow dependency, there can be situations where coupling on a higher harmonic has real advantages. In particular, the choice is dependent on the spectrum of the electromagnetic power sources available, since the total IFEL interaction strength depends also on the input driving power (as K_l), and a smaller coupling strength is easily compensated by a higher level of input power.

In an FEL seeding scenario, the possibility offered by harmonic seeding—seeding with a harmonic of the undulator resonant frequency—can be an interesting shortcut towards shorter wavelength radiation produced with relatively low energy accelerators. One scheme considered for FEL seeding is to use the higher harmonics produced when focusing an intense laser beam on a gas target [25]. The output radiation has a spectrum with peaks at the odd harmonics of the input radiation. It is then relatively easy, by selecting a particular component of the frequency spectrum, to switch to a shorter wavelength of the seed and of the electron beam microbunches periodicity, without changing the beam energy and/or undulator parameters.

Another interesting possibility that we can analyze in the framework of the higher harmonic IFEL is to drive the IFEL with many different harmonics at the same time to obtain shorter microbunches. It is known in fact, that the shortest microbunch length achievable with an IFEL buncher is limited by the nonlinearities of the IFEL longitudinal lens [26]. The cosinelike ponderomotive potential characterizing the IFEL dynamics effectively gives rise to longitudinal emit-

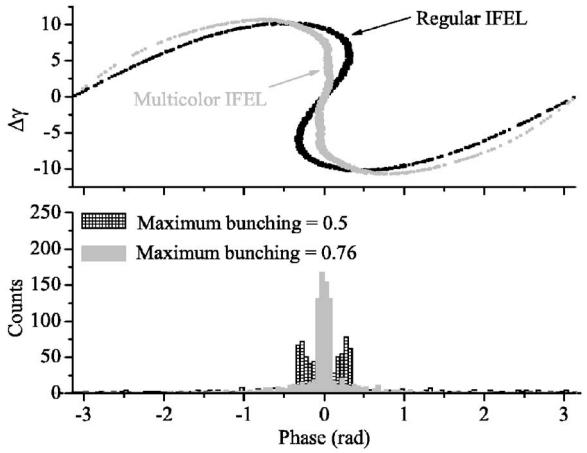

FIG. 8. Longitudinal phase space and bunching factor improvements for a multicolor-driven IFEL.

tance growth that limits the microbunch length to about 1/10 of the laser wavelength. If the IFEL buncher is used only to impart an energy modulation on the beam that a magnetic chicane dispersive section subsequently converts into a density modulation, then the IFEL aberrations can be traded against the aberrations of the (more easily fabricated) chicane, potentially leading to shorter bunches. In the IFEL-only case, which is characterized by a full microbunched beam already at the end of the undulator, an aberration-free dynamics would correspond to an equation of motion with linear forces (corresponding to a parabolic potential), where the final microbunch length is determined only by the initial longitudinal emittance, which is preserved in the interaction.

We can consider the use of different laser frequencies to linearize the dynamical evolution of the electron longitudinal phase space. In particular, a parabolic function can be Fourier expanded as

$$V_{\text{ideal}}(\psi) = 1 - \frac{\psi^2}{2} = \frac{a_0}{2} + \sum_{n=1}^{+\infty} a_n \cos(n\psi), \tag{26}$$

with the coefficients a_n being the Fourier components of the parabolic potential. Using a multicolor driver for the IFEL interaction with ratios of the harmonics a_n/JJ_n we may obtain a longitudinal phase space evolution that is a better approximation to the ideal case and consequently obtain shorter bunches out of the IFEL interaction.

In Fig. 8 we show the longitudinal phase spaces for an IFEL interaction driven with five harmonics with optimal ratios of intensities (gray), and for a case where only the fundamental frequency is present (black). A figure of merit for the microbunching is the bunching factor defined as $B = \Sigma e^{i\theta_i}/N$, where N is the number of particles in the beam. This quantity is equal to 0 for a uniformly distributed beam and tends to 1 for a perfectly microbunched beam and it represents the coherence enhancement factor for the radiation emitted by the beam at the microbunching wavelength. In the case where only the fundamental frequency drives the IFEL, the bunching parameter reaches a value of 0.5. In the multicolor IFEL case, the longitudinal phase space appears more linear, and the bunching parameter correspondingly goes up to 0.75. The application requirements of the microbunched electron beam should determine if the improvements achieved with the multicolor IFEL buncher are worth the experimental complexity of injecting into the undulator multiple frequency components. We note that the creation of harmonics of intense, near-optical wavelength lasers is accomplished straightforwardly through use of harmonic conversion in crystalline materials [27]. For shorter wavelengths, one may consider gas target-based conversion, as mentioned above.

VI. STRONGLY TAPERED UNDULATORS AND COMPARISON WITH EXPERIMENTAL RESULTS

Let us consider now a final situation where the higher harmonic IFEL interaction is relevant, a high-gradient high-gain IFEL accelerator module. For this device, the undulator magnet is strongly tapered to maintain the resonance condition along the interaction region with the accelerating particles. The tapering of the undulator defines multiple resonant curves, one for each harmonic number. If there is sufficient laser intensity, electrons can be trapped in each of the stable longitudinal phase space regions and accelerated along the corresponding resonant curve. To maximize the energy exchange, the undulator is usually built in such a way that the design trajectory corresponds to the fundamental resonant energy.

In an ideal IFEL accelerator, the injected beam is microbunched with the periodicity of the laser wavelength and all the particles are trapped inside the ponderomotive bucket separatrix. In this case the energy spectrum of the beam remains relatively narrow and peaked around the design resonant energy. Practically, there are a number of reasons to find particles along the undulator at energies much different than the design resonant energy. In particular, even though quite high trapping efficiency has been experimentally demonstrated, it is effectively impossible to inject a train of bunched electrons phase-locked with the driving laser with 100% trapping efficiency. Consequently some or most of the injected particles (depending on the initial capturing section) do not get trapped inside the design resonant ponderomotive bucket. Moreover, along the interaction region, trapped eletrons can become detrapped because of trajectory misalignment, or because of a mismatch between the design tapering and the available ponderomotive gradient. All the nontrapped, weakly interacting electrons propagate in the undulator with energies smaller than the design resonant value, until at some point along the interaction region their energy coincides with the monotonically increasing energy associated with a higher harmonic resonant curve. At this point significant energy exchange between the particles and the laser can occur again via the higher harmonic IFEL interaction.

This was in fact the situation of the Neptune IFEL experiment. For a more detailed description of the experiment, we refer to [7]. In this high-gradient high-gain experiment, the 50 cm long undulator was strongly tapered both in period and amplitude to accept electrons initially at 14.5 MeV and

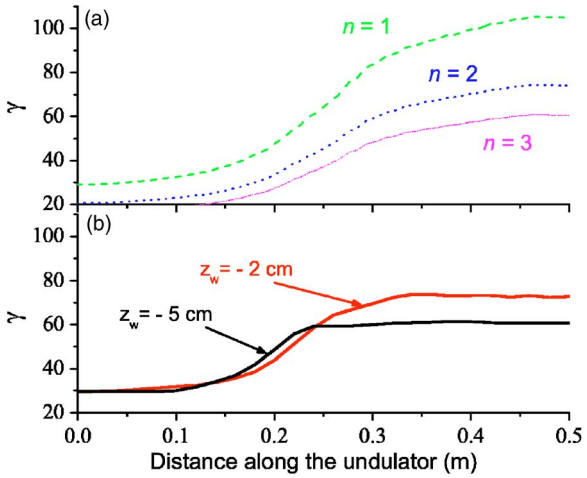

FIG. 9. (Color online) Resonant energies for the first three harmonic IFEL interactions along the Neptune IFEL undulator, and evolution of the simulated electron beam maximum energy for two different laser focus positions.

accelerate them to over 50 MeV. In Fig. 9 we show the first three higher harmonic resonant energies along the undulator.

Because of a mismatch between the design and real laser intensity distribution along the undulator, the device had to be operated with the laser focus moved upstream of its nominal position at the center of the undulator. In Fig. 10 we show two measured energy spectra (histograms in Fig. 10) obtained with the laser focus at two different positions, respectively 5 and 2 cm upstream of the undulator midpoint. The laser power for these shots was 350 and 400 GW, respectively. The IFEL energy spectra are reconstructed from single-shot calibrated images of the fluorescent screen located at the exit of a wide band spectrometer. The dispersion $\delta=\Delta x/\Delta p$ is not constant along this screen, and it grows from 1 cm/MeV for the lower energies end to 4 cm/MeV for higher energies. The resolution is sufficient to fully distinguish different peaks in the high energy part of the spectra. The camera noise level sets a minimum detectable charge density. Converting this threshold with the use of the screen calibration into the graph units, we obtain a minimum detection threshold below 10 counts.

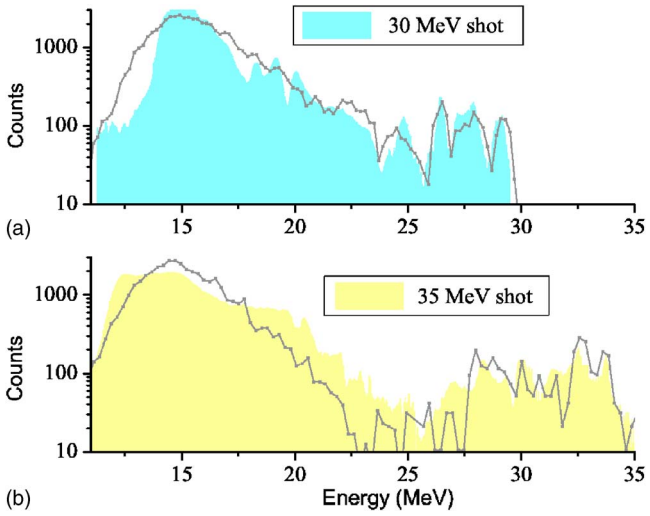

FIG. 10. (Color online) Measured and simulated output energy spectrums for the Neptune IFEL accelerator experiment for two different laser focus positions. The simulated spectra have been normalized to the same area as the measured ones.

When using the experimental parameters, TREDI simulations (lines in Fig. 10) agree quite well with the measured energy spectra, especially in reproducing the peaked structure appearing in the high energy side. Experimentally, the relative amplitudes of the peaks oscillated shot-to-shot changing with the fluctuating input laser power, but the position of the peak centroids was very reproducible, ruling out the possibility of being caused by microstructures present in the electron beam or in the laser beam.

To have an insight on this, we can follow the evolution of the maximum-energy particle in the simulations and obtain the solid curves shown in Fig. 9(b). A few cm after the undulator center, the particles fall off the resonance curve [first harmonic resonance, $n=1$ dashed curve in Fig. 9(a)] because the driving laser intensity has decreased below the trapping threshold. Some distance later, their energy is a factor of $\sqrt{2}$ less than the first harmonic resonant energy at that point of the undulator, and therefore the electrons are resonant with the $n=2$ dotted curve and can exchange energy with the 10.6 μm photons via the second harmonic IFEL interaction. Later on, the electrons have energies such that energy exchange with the laser can start even via the stronger third harmonic coupling ($n=3$ dash-dotted curve). In the Neptune IFEL case, though, the tapering of the undulator is designed to match the coupling and the intensity of the first harmonic, so the particles cannot be accelerated along the higher harmonic resonant curves because of the lack of a stable accelerating region in the phase space. A small energy exchange takes place, enough to modulate the final energy distribution and this corresponds to the peaked microstructure observed reproducibly in the experimental spectrum.

Different factors contribute to the second harmonic coupling observed in the Neptune IFEL experiment. This experiment was characterized by the fact that the laser beam was coupled in the undulator with a short Rayleigh range compared to the undulator length. Thus three-dimensional effects dominated the dynamics of the IFEL interaction. In particular, the laser waves have an intrinsically large angular spread characterized by the diffraction angle. Unavoidable angular misalignments, as well as trajectory offsets of the electron and the laser beams, possibly contributed to the second harmonic interaction coefficient. Moreover, the laser mode used in the experiment is not a purely Gaussian TEM_{00} mode, as it was assumed in the design and in the simulations. After passing in the final amplifier, the transverse profile of the CO_2 pulse experimentally shows a supersaturated Gaussian profile, with a content of different higher order Hermite-Gaussian modes. The higher harmonic interaction is weak, but the energy exchange is significant because the laser is still somewhat intense ($>10^{10}$ W/cm^2) and the wiggling parameter K is large at the end of the undulator.

It is interesting to compare two different experimental cases. In the 30 MeV case [Fig. 10(a)], the structure of the peaks is more pronounced. In this case, in fact, the particles fall off the first resonant curve at $z=25$ cm (see solid curves

in Fig. 9) and the laser wave can exchange energy with the electrons via the second and third harmonic interaction for a longer distance thus imparting a stronger energy modulation on the phase space. In the 35 MeV shot case [Fig. 10(b)], the higher harmonic interaction is turned on only in the last 10–15 cm of the undulator in a region where the laser intensity is weaker, so the induced energy modulation is reduced.

VII. CONCLUSIONS

We have expanded the theoretical description of the IFEL interaction, including one aspect often overlooked in previous models, the interaction inside an undulator magnet of an electron beam and a laser wave of a frequency that is a higher harmonic of the undulator fundamental resonant frequency. We have calculated the IFEL coupling coefficients and explored the possible configurations where this coupling has the strongest effect. The suppression of the even harmonic coupling is a reflection of the fact that the on-axis spontaneous radiation spectrum of a planar undulator does not contain even harmonics of the undulator fundamental resonant frequency. A nonvanishing even-harmonic coupling can be achieved when the transverse symmetry of the IFEL interaction is broken, allowing net acceleration or deceleration to occur over an undulator period at such harmonics.

In some cases, the strength of the higher harmonic IFEL coupling can be comparable to the fundamental coupling and efficient energy exchange can take place in higher harmonically tuned undulators. In general, this offers a new degree of freedom when designing systems capable of coupling high power laser beams and relativistic electron beams. The Neptune IFEL high-gain high-gradient experiment offers an experimental example where the higher harmonic IFEL interaction played an important role and produced observable effects on the measured electron beam energy spectrum.

ACKNOWLEDGMENTS

We acknowledge the helpful support of Dr. Tochitsky and the Neptune Laboratory team. One of us (P. M.) wishes to thank Professor Mattioli for his encouragement and interesting discussions. This work was supported by U.S. Dept. of Energy Grant No. DE-FG03-92ER40693 and by Istituto Nazionale di Fisica Nucleare sez. Roma 1

[1] R. Palmer, J. Appl. Phys. **43**, 3014 (1972).
[2] E. D. Courant, C. Pellegrini, and W. Zakowicz, Phys. Rev. A **32**, 2813 (1985).
[3] N. M. Kroll, P. L. Morton, and M. N. Rosenbluth, IEEE J. Quantum Electron. **QE-17**, 1436 (1981).
[4] Y. Liu *et al.*, Phys. Rev. Lett. **80**, 4418 (1998).
[5] W. Kimura *et al.*, Phys. Rev. Lett. **86**, 4041 (2001).
[6] W. Kimura *et al.*, Phys. Rev. Lett. **92**, 054801 (2004).
[7] P. Musumeci *et al.*, Phys. Rev. Lett. **94**, 154801 (2004).
[8] L. H. Yu *et al.*, Science **289**, 932 (2000).
[9] C. E. Sung *et al.*, in *Advanced Accelerator Concepts: Eleventh Workshop*, edited by V. Yakimenko, AIP Conf. Proc. No. 737 (AIP, Melville, NY, 2004), p. 922.
[10] C. M. S. Sears, E. Colby, and C. Barnes, in *Advanced Accelerator Concepts: Eleventh Workshop*, edited by V. Yakimenko, AIP Conf. Proc. No. 737 (AIP, Melville, NY, 2004), p. 342.
[11] W. Kimura *et al.*, in *Advanced Accelerator Concepts: Eleventh Workshop*, edited by V. Yakimenko, AIP Conf. Proc. No. 737 (AIP, Melville, NY, 2004), p. 251.
[12] W. M. Fawley *et al.*, in *Proc. of 25th Free-Electron-Laser Conference, Trieste, Italy* (Comitato Conferenze Elettra, Trieste, Italy, 2004).
[13] M. S. Zolotorev and A. A. Zholents, Phys. Rev. E **50**, 3087 (1994).
[14] A. A. Zholents and M. S. Zolotorev, Phys. Rev. Lett. **76**, 912 (1996).
[15] Z. Huang and K. J. Kim, Phys. Rev. E **62**, 7295 (2000).
[16] W. B. Colson, IEEE J. Quantum Electron. **QE-17**, 1417 (1981).
[17] A. Tremaine *et al.*, Phys. Rev. Lett. **88**, 204801 (2002).
[18] W. B. Colson, G. Dattoli, and F. Ciocci, Phys. Rev. A **31**, 828 (1985).
[19] M. J. Schmitt and C. J. Elliott, Phys. Rev. A **34**, 4843 (1986).
[20] A. E. Siegman, *Lasers* (*University Science Books*, Mill Valley, CA, 1990).
[21] P. Musumeci and C. Pellegrini, in *Advanced Accelerator Concepts: Ninth Workshop*, edited by P. L. Colestock, AIP Conf. Proc. No. 569 (AIP, Melville, NY, 2000), p. 249.
[22] L. Giannessi, P. Musumeci, and M. Quattromini, Nucl. Instrum. Methods Phys. Res. A **436**, 443 (1999).
[23] F. Zhou, D. B. Cline, and W. D. Kimura, Phys. Rev. ST Accel. Beams **6**, 054201 (2003).
[24] L. C. Steinhauer and W. D. Kimura, Phys. Rev. ST Accel. Beams **2**, 081301 (1999).
[25] G. Lambert *et al.*, in *Proc. of 25th Free-Electron-Laser Conference, Trieste, Italy* (Comitato Conferenze Elettra, Trieste, Italy, 2004).
[26] P. Musumeci *et al.*, in *Proc. of the International Conference on Lasers 2001, Tucson, AZ* (STS Press, McLean, VA, 2002), p. 41.
[27] G. G. Gurzadian, V. G. Dmitriev, and N. D. Nikogosian, *Handbook of Nonlinear Optical Crystals* (Springer-Verlag, Berlin, 1999).